PALEOCEANOGRAPHY, VOL. 12, NO. 2, PAGES 191-205, APRIL 1997

The California Current of the last glacial maximum: Reconstruction at 42°N based on multiple proxies

Joseph Ortiz[1] and Alan Mix

College of Oceanic and Atmospheric Sciences, Oregon State University, Corvallis

Steve Hostetler

U.S. Geological Survey at U.S. Environmental Protection Agency, Corvallis, Oregon

Michaele Kashgarian

Lawrence Livermore National Laboratory, Livermore, California

Abstract: Multiple paleoceanographic proxies in a zonal transect across the California Current near 42°N record modern and last glacial maximum (LGM) thermal and nutrient gradients. The offshore thermal gradient, derived from foraminiferal species assemblages and oxygen isotope data, was similar at the LGM to that at present (warmer offshore), but average temperatures were 3.3° ±1.5°C colder. Observed gradients require that the sites remained under the southward flow of the California Current, and thus that the polar front remained north of 42°N during the LGM. Carbon isotopic and foraminiferal flux data suggests enhanced nutrients and productivity of foraminfera in the northern California Current up to 650 km offshore. In contrast, marine organic carbon and coastal diatom burial rates decreased during the LGM. These seemingly contradictory results are reconciled by model simulations of the LGM wind- field, which suggest that wind stress curl at 42°N (and thus open-ocean upwelling) increased, while offshore Ekman transport (and thus coastal upwelling) decreased during the last ice age. The ecosystem of the northern California Current during the LGM approximated that of the modern Gulf of Alaska. Cooling and production in this region was thus driven by stronger open-ocean upwelling and/or southward flow of high-latitude water masses, rather than by coastal upwelling.

Introduction

We report here on conditions in the northern California Current during the last glacial maximum (LGM). Previous studies suggest that NE Pacific surface waters cooled by 2°-4°C [*Moore*, 1973; *Moore et al.* 1980] and that export production decreased relative to present values [*Lyle et al.* 1992; *Sancetta et al.* 1992]. These past studies were limited to a few cores at different latitudes, which precludes resolution of water mass flows. To resolve regional currents, we focus on zonal temperature and nutrient structures at 42°N in a transect of 10 cores that span the California Current from 125°W to 134°W. To evaluate causes of oceanographic change, we compare geologic data with local wind forcing simulated with a regional climate model.

Our transect, located between Cape Blanco and Cape Mendocino, is sensitive to southward translation of the polar front zone (the boundary between the subarctic and subtropical gyres) because it is near the southern boundary of the transition zone between these gyre systems. Today, year-round flow is southward (Figure 1) and near-coastal upwelling is strong in summer. By reconstructing the LGM zonal thermal gradient here we infer direction in the surface water circulation and thus put limits on polar front movements.

Had the LGM polar front moved south of these sites, flow across the transect would have been northward, similar to the Alaskan Stream off British Columbia today. This would be indicated by warmer, more nutrient-depleted water near the coast than offshore. If the LGM polar front stayed to the north, our sites would have remained under a southward flowing California Current, with colder nutrient-enriched water near the coast and warmer, more nutrient-depleted waters offshore.

Methods

Foraminiferal Faunas: Temperature and Productivity Estimates

We identified foraminiferal species percentages in the >150-μm size class using standard CLIMAP taxonomic categories [*Parker*, 1962: *Bé*, 1977] with one exception. In this study, we do not recognize the "*Neogloboquadrina pachyderma - neogloboquadrina dutertrei (P-D) intergrade*" category of *Kipp* [1976].

We compare modern foraminiferal faunas from sediment traps and plankton tows with local fossil assemblages obtained from well- preserved LGM sediments (Table 1). Core top faunas in this area are highly dissolved and thus unusable for our study [*Karlin et al.* 1992; *Zahn et al.* 1991b; *Lyle et al.* 1992].

[1]Now at Lamont-Doherty Earth Observatory of Columbia University, Palisades, New York.

Paper number 96PA03165.
0883-8305/97/96PA-03165$12.00

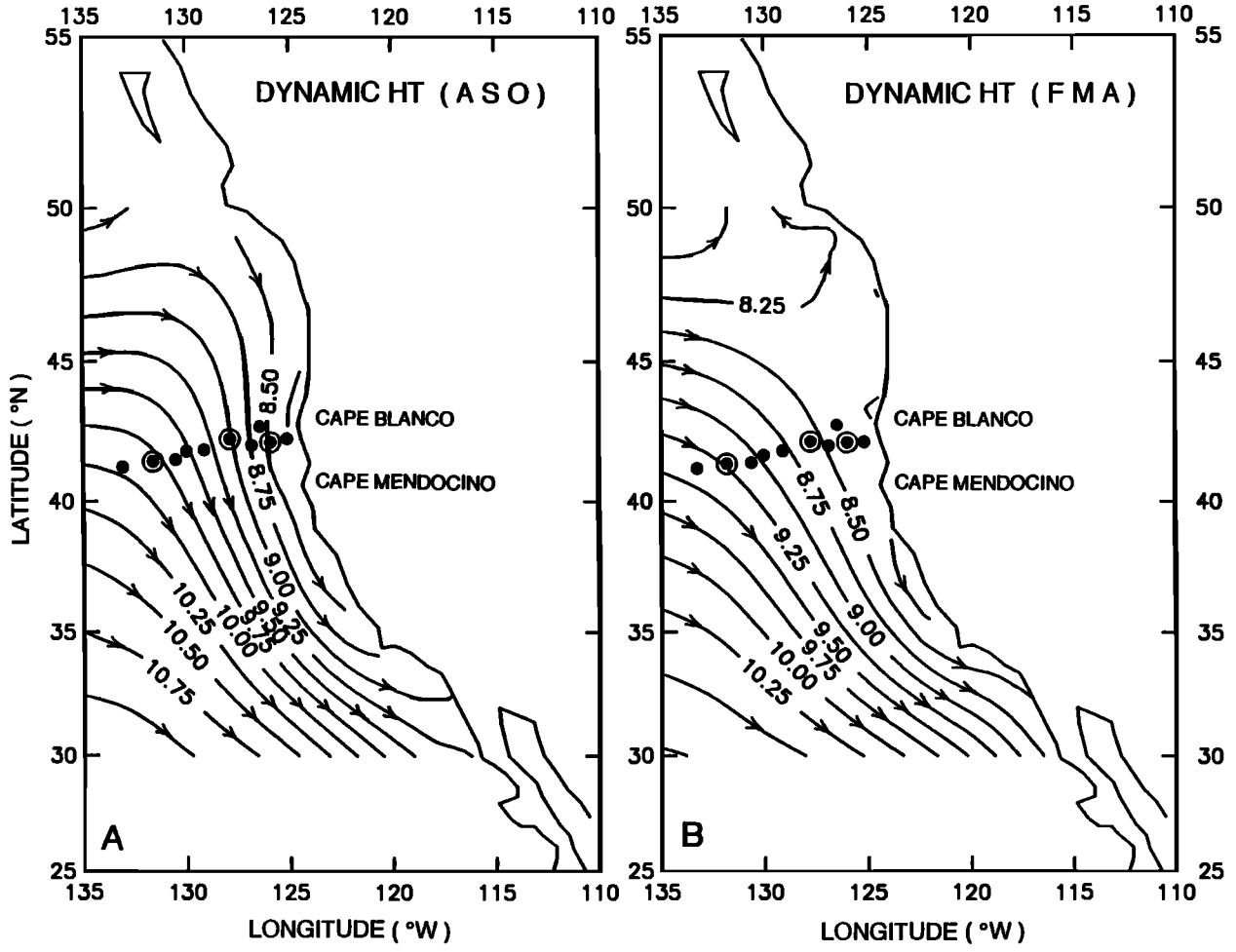

Figure 1. Locations of the sediment cores (solid circles) and sediment trap moorings (solid circles surrounded by circles) across the California Current near 42°N. Contours are the climatic average dynamic height field relative to 500 m in units of geopotential ($m^2 s^{-2}$). Geopotential is a measure of the geostrophic flow during (a) August, September, and October and (b) February, March, and April, using data from *Levitus* [1982]. Closer contours denote faster currents; arrows show the direction of flow.

Table 1. Multitracers Core and Trap Locations

Name	Age Control[a]	Latitude, °N	Longitude, °W	Depth, m	Length, cm
		Sediment Cores			
6706-2	type 1 and 2	42.16	124.94	1120	390
W8709A-13PC	type 3	42.12	125.75	2717	872
W8809A-53GC	type 3	42.75	126.26	2408	258
W8809A-21GC	type 3	42.14	126.91	2799	255
W8709A-08PC	type 3	42.26	127.68	3111	875
W8809A-29GC	type 3	41.80	129.00	3136	266
W8809A-31GC	type 3	41.68	130.01	3136	266
W8909A-57GC	type 3	41.58	130.62	3330	252
W8709A-01BC	type 1	41.54	131.96	3680	48
W8909A-48GC	type 1	41.33	132.67	3670	251
		Sediment Traps			
Nearshore trap	N/A	42.09	125.77	1000	N/A
Midway trap	N/A	42.19	127.58	1000	N/A
Gyre trap	N/A	41.54	132.02	1000	N/A

[a]Three methods of age control are used: Type 1 is carbonate stratigraphy, type 2 is conventional ^{14}C dating of bulk organic matter [from *Spigai*, 1971], and type 3 is AMS ^{14}C on planktic or benthic foraminifera.

Foraminiferal sediment trap fluxes are from *Ortiz and Mix*, [1992], but were modified by grouping *P-D* intergrade with *Neogloboquadrina dutertrei*.

Paleotemperature estimates use a version of the modern analog method tested on both core top and sediment trap faunas [*Ortiz and Mix*, this issue]. This method yields unbiased sea surface temperature (SST) estimates with an RMS error of 1.5°C for the core top data set. Additional checks include (1) radiolarian paleotemperature estimates [*Sabin and Pisias*, 1996], and (2) $\delta^{18}O$ measurements of *G. bulloides*.

We infer LGM nutrient content and foraminiferal productivity from (1) $\delta^{13}C$ gradients of *G. bulloides* across the transect and (2) shell accumulation rates of the heterotrophic planktonic foraminifera. Modern shell accumulation rates are from sediment trap fluxes, subject to little or no dissolution. LGM faunas are well preserved, but possible losses due to partial dissolution imply that preserved accumulation rates are minimum estimates for original shell fluxes. We assume a relationship between water column nutrient content and shell fluxes because nutrients control the food supply of heterotrophic foraminifera [*Ortiz* 1995; *Ortiz et al.* 1995; *Ortiz and Mix*, 1992]. Given a life span of about 1 month [*Hemleben et al.*1988], foraminifera like other zooplankton can respond to changes in prey abundance related to upwelling events of several weeks duration, in addition to advective changes on longer timescales [*Barnard*, 1994].

Age Models

Age models are needed both for synoptic sampling of the LGM and for calculating sediment accumulation rates. Core locations are given in Table 1. Stratigraphic control includes calcium carbonate percentages, oxygen isotope stratigraphy, and radiocarbon dating. The LGM horizon, defined here as between calendar-corrected radiocarbon ages of 16-22 ka, is associated with high $\%CaCO_3$ in cores east of 129°W (Figure 2) [*Lyle et al.* 1992]. Farther west, the carbonate high is broader, and the LGM horizon is chosen near the younger end of the carbonate high. Carbonate percentage data are in Table 2.

Radiocarbon dates on foraminifera come from *Lyle et al.* [1992], *Gardner et al.* [this issue], and the present study (Table 3). Dates from consecutive 2-5 cm intervals that were not statistically independent were averaged. Reservoir corrections, needed to adjust for the apparent ^{14}C age of the water in which the foraminifera lived, assume that benthic foraminifera calcified in North Pacific deep waters with $\Delta^{14}C$ = -250‰ [*Östlund et al.* 1987], as defined on the $\Delta^{14}C$ scale of *Stuiver and Polach* [1977]. The benthic reservoir correction is thus 2380 years, using the "Godwin" ^{14}C half-life of 5730 years [*Faure*, 1977]. Subtracting the average ^{14}C age difference between benthic and planktonic foraminifera in the same samples from the assumed benthic reservoir correction, we find a planktonic reservoir correction of 718 years. This estimate is virtually

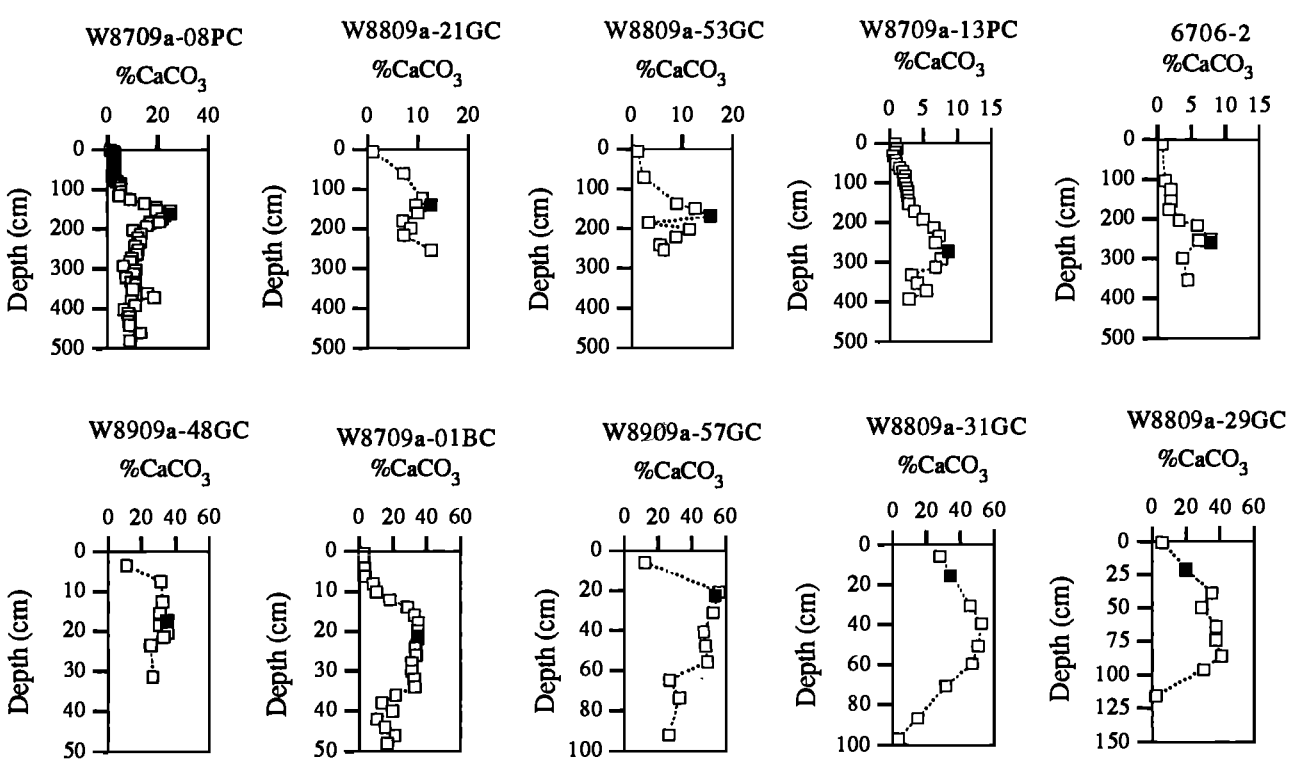

Figure 2. Percent carbonate stratigraphies for the 10 cores in the transect, ordered by distance from the coast: 6706-2 is closest to the coast, while W8909A-48GC is farthest offshore. solid squares mark the last glacial maximum (LGM) samples identified by carbonate stratigraphy and AMS-^{14}C dating. Some carbonate data for 6706-2 are from *Spigai* [1971]. Carbonate data for W8709A-13PC, 13TC, W8709A-8PC, TC, and W8709A-1BC from *Lyle et al.* [1992].

Table 2. Carbonate Stratigraphies for the Multitracers Cores

Depth, cm	$CaCO_3$, %	Depth, cm	$CaCO_3$, %	Depth, cm	$CaCO_3$, %	Depth[a], cm	$CaCO_3$, %
6706-2PC		*W8809A-53GC*		*W8809A-21GC*		*W8809A-29GC*	
11.5	0.72	5.5	1.19	5.5	0.98	135.5	6.05
102.5	1.06	70.5	2.36	60.5	7.16	155.5	19.91
124.5	1.95	137.5	8.88	123.5	10.80	173.5	34.92
152.5	1.95	150.5	12.44	140.5	9.56	184.5	29.02
175.5	1.68	170.5	15.52	160.5	9.91	198.5	37.71
202.5	3.12	185.5	3.25	180.5	6.93	208.5	37.53
215.5	5.84	202.5	11.37	198.5	8.46	220.5	40.48
249.5	7.94	222.5	8.73	216.5	7.14	230.5	30.21
252.5	6.07	241.5	5.55	254.5	12.61	250.5	1.85
298.5	3.65	255.5	6.30				
352.5	4.42						
W8809A-31GC		*W8909A-57GC*		*W8909A-48GC*			
5.5	27.77	5.5	11.95	3.5	10.72		
30.5	45.58	20.5	55.67	7.5	31.20		
39.5	52.38	30.5	52.35	12.5	32.18		
50.5	50.32	40.5	46.69	15.5	30.49		
59.5	46.78	47.5	47.75	18.5	30.49		
70.5	31.22	55.5	48.76	20.5	34.92		
86.5	14.83	64.5	26.41	21.5	32.98		
96.5	2.87	73.5	32.25	23.5	25.26		
122.5	52.54	91.5	26.08	31.5	26.39		

[a]Core top occurs at approximately 135 cm depth due to double coring.

identical to that of *Zahn et al.* [1991a]. The benthic-planktonic age comparison in five samples of up to 25,000 ^{14}C years suggests that the average reservoir age of the surface water was roughly constant over that time interval. We thus subtracted 718 years from each of the planktonic foraminiferal dates, and 2380 years from each of the benthic foraminiferal dates, for reservoir corrections. Reservoir corrections on bulk organic carbon dates are calculated to align their ages with those of the reservoir-corrected calcite dates. This empirical correction (4300 years) is larger than any reasonable open-ocean reservoir age. It implies that some older reworked material is present as part of the bulk organic carbon. The conclusions of this study would not change if the organic carbon dates were excluded.

The reservoir-corrected benthic and planktonic ages of >5000 ^{14}C years were converted to calendar age (Table 3) using the nonlinear relationship of *Bard et al.* [1992]:

$$\text{calendar age} = -5.85 \times 10^{-6} (\text{conventional } ^{14}C \text{ age})^2 + 1.39 (\text{convential } ^{14}C \text{ age}) - 1807. \quad (1)$$

The term "conventional ^{14}C age" refers to ^{14}C ages in radiocarbon years which have been reservoir corrected. Data used to construct the non-linear relationship of *Bard et al.* [1992] are published by *Bard et al.* [1993]. *Bard et al.* [1992] also present a linear relationship for use with ^{14}C dates from 9 to 18 ka. Differences between these two relationships (linear minus nonlinear) range from 5 to 360 years. The differences between the two equations are thus comparable to the 2σ errors of our dates. Likewise, calendar correction factors from equation (1) for ages of <5000 ^{14}C years are close to the precision of the AMS-^{14}C dates. We did not attempt any correction factors for these relatively young dates. E. Bard (personal communication, 1996) considers equation (1) appropriate for samples between ^{14}C ages of 10,000 and 22,000 years, and thus well constrained for calendar correction of our LGM samples.

Stable Isotopic Measurements

Oxygen ($\delta^{18}O_c$) and carbon ($\delta^{13}C_c$) stable isotopes were measured at Oregon State University using a Finnigan MAT-251 stable isotope mass spectrometer, equipped with an Autoprep Systems automated carbonate preparation device. Each sample consisted of 12 *G. bulloides* shells (300- to 355-μm size) collected from the LGM horizon in 10 sediment cores. Isotopic data use the standard isotopic delta notation (δ), in per mil (‰) relative to the Pee Dee belemnite (PDB) scale. Calibration to PDB was done through the NBS-19 and NBS-20 standards of the National Institute of Standards and Technology. External precision estimates for $\delta^{18}O$ and $\delta^{13}C$, based on replicate analyses of local calcite standards, are ±0.08 and ±0.04‰, respectively.

Regional salinity (S) and the oxygen isotopic composition of water ($\delta^{18}O_w$) are positively correlated [*Craig and Gordon*, 1965]. Because $\delta^{18}O_c$ is a function of both temperature (T) and $\delta^{18}O_w$, lines of constant $\delta^{18}O_c$ plotted in *T-S* space approximate lines of constant density. This relationship holds over small spatial scales where it is safe to assume that the regional salinity - $\delta^{18}O_w$ slope and intercept are constant. We thus use the slope of $\delta^{18}O_c$ along the 42°N transect as a crude measure of the LGM density gradient. This gradient yields an estimate of surface water flow direction and magnitude, assuming geostrophy.

Table 3. AMS-^{14}C dates for the Multitracers Cores

Core	Sample Depth,[a] cm	Material	Source	Raw AMS-^{14}C,[b,c] ka	Raw AMS-^{14}C Error, ka	Reservoir Corrected Age,[d] ka	Calendar Age, ka
W8709A-8TC	27-28	bulk Corg	*Lyle et al.* [1992]	6.94	0.11	2.64	2.64
W8709A-8TC	77-78	bulk Corg	*Lyle et al.* [1992]	10.44	0.13	6.14	6.51
W8709A-8TC	125-126	bulk Corg	*Lyle et al.* [1992]	15.30	0.21	11.00	12.78
W8709A-8TC	120-130	planktics	*Lyle et al.* [1992]	12.28	0.25	11.56	13.48
W8709A-8TC	150-160	planktics	*Lyle et al.* [1992]	15.85	0.29	15.13	17.88
W8709A-8PC	20-25	planktics	*Lyle et al.* [1992]	15.76	0.40	15.04	17.78
W8709A-8PC	50-55	planktics	*Lyle et al.* [1992]	18.49	0.28	17.77	21.05
W8709A-8PC	80-85	planktics	*Lyle et al.* [1992]	20.92	0.38	20.20	23.88
W8709A-8PC	111-116	planktics	*Lyle et al.* [1992]	21.16	0.61	20.44	24.16
W8709A-13PC	25-30	planktics	*Gardner* et al. [this issue]	7.00	0.23	6.28	6.69
W8709A-13PC	95-100	mixed benthics	*Gardner et al.* [this issue]	11.01	0.36	8.63	9.76
W8709A-13PC	125-130	mixed benthics	*Gardner et al.* [this issue]	11.51	0.33	9.14	10.40
W8709A-13PC	125-130	planktics	*Gardner et al.* [this issue]	9.96	0.23	9.24	10.54
W8709A-13PC	195-200	mixed benthics	*Gardner et al.* [this issue]	14.63	0.39	12.25	14.34
W8709A-13PC	195-200	planktics	*Gardner et al.* [this issue]	13.43	0.19	12.71	14.91
W8709A-13PC	220-225	mixed benthics	*Gardner et al.* [this issue]	15.86	0.50	13.48	15.87
W8709A-13PC	220-225	planktics	*Gardner et al.* [this issue]	14.04	0.28	13.32	15.67
W8709A-13PC	270-275	planktics	*Lyle et al.* [1992]	15.27	0.22	14.55	17.18
W8709A-13PC	300-305	mixed benthics	*Gardner et al.* [this issue]	18.49	0.38	16.12	19.07
W8709A-13PC	300-305	planktics	*Gardner et al.* [this issue]	16.87	0.27	16.15	19.12
W8709A-13PC	330-335	planktics	*Lyle et al.* [1992]	18.37	0.27	17.65	20.90
W8709A-13PC	390-395	planktics	*Lyle et al.* [1992]	19.82	0.61	19.10	22.61
W8709A-13PC	400-405	mixed benthics	*Gardner et al.* [this issue]	24.05	1.53	21.67	25.57
W8709A-13PC	400-405	planktics	*Gardner et al.* [this issue]	21.96	0.49	21.24	25.08
W8809A-21GC	175-176	*G. bulloides*	this study	20.92	0.16	20.20	23.89
W8809A-31GC	5-6	*G. bulloides*	this study	16.10	0.17	15.38	18.19
W8809A-31GC	12-13	*G. bulloides*	this study	16.54	0.10	15.82	18.72
W8809A-31GC	39-40	*G. bulloides*	this study	31.37	0.50	30.65	35.30
W8809A-31GC	65-66	*G. bulloides*	this study	36.01	1.26	35.29	39.96
W8809A-29GC	160-161	*G. bulloides*	this study	20.72	0.14	20.00	23.66
W8809A-29GC	220-221	*G. bulloides*	this study	43.35	2.37	42.63	46.82
W8809A-29GC	232-233	*G. bulloides*	this study	>45.60	N/A	>44.88	>48.80
W8809A-53GC	140-141	*G. bulloides*	this study	13.43	0.11	12.71	14.92
W8809A-53GC	170-171	*G. bulloides*	this study	15.03	0.80	14.31	16.89
W8809A-53GC	200-201	*G. bulloides*	this study	18.13	0.11	17.41	20.62
W8909A-57GC	14-15	*G. bulloides*	this study	15.64	0.80	14.92	17.63
W8909A-57GC	20-21	*G. bulloides*	this study	15.75	0.90	15.03	17.77
W8909A-57GC	58-59	*G. bulloides*	this study	43.65	1.16	42.93	47.09

[a] W8709A-8PC overpenetrated by 140 cm [*Lyle et al.*, 1992]. This value must be added to the tabulated depth listed here for samples from W8709A-8PC to determine true depth below seafloor. W8809A-29GC double cored by 135 cm based on visual inspection and AMS dating results, 135 cm must be subtracted from the values tabulated here to determine true depth below sea floor.

[b] Raw data from *Lyle et al.* [1992] were originally published in reservoir corrected form. Revised calendar corrections for these samples are based on the methods described in the text. Dates from *Gardner et al.* [this issue] were obtained from J.V. Gardner prior to publication. Values presented here are averages of two consecutive 2.5 cm samples. The sum of the individual errors for each sample are listed in the table.

[c] Calculated using the Libby half-life for ^{14}C.

[d] The planktic and mixed benthic dates were reservoir corrected as described in the text. Following *Lyle et al.* [1992], the bulk Corg dates were offset by 4.3 ka relative to the reservoir corrected planktic dates.

We estimate the oxygen isotopic composition of calcite in equilibrium with the water column ($\delta^{18}O_c$) using T and $\delta^{18}O_w$ as inputs to the paleotemperature equation of *Epstein et al.* [1953]. For modern conditions we use SST and surface salinity from *Levitus* [1982] as the inputs. Conversion of salinity to $\delta^{18}O_w$ uses the northeast Pacific relationship of *Zahn et al.* [1991a]:

$$\delta^{18}O_w = 0.405(\text{salinity}) - 14.01 \text{ ‰}. \quad (2)$$

To estimate the relative magnitude of the LGM SST and surface salinity changes recorded in $\delta^{18}O_c$, we assume (1) an LGM ice volume $\delta^{18}O$ effect of +1.3‰ relative to present values [e.g., *Fairbanks*, 1989; *Mix*, 1987], (2) a salinity-$\delta^{18}O_w$ slope the same as at present, and (3) a constant depth habitat for *G. bulloides* (0- 30 m in these sites at present [*Ortiz et al.* 1995]. The third assumption is the weakest. In the Gulf of Alaska, *G. bulloides* resides between 100 and 150 m [*Miles*, 1973; *Zahn et al.* 1991a]. This depth range is within the main pycnocline, below the base of the mixed layer and above the North Pacific halocline. According to *Zahn et al.* [1991a], this subsurface habitat makes the $\delta^{18}O$ of late holocene *G. bulloides* up to 1‰ enriched relative to seasonally weighted surface water $\delta^{18}O_c$ for the Gulf of Alaska. If the relationship to the pycnocline is functional, a shift to a similar depth habitat during the LGM

could result in a $\delta^{18}O$ offset of up to 1‰ during the LGM. Thus any downward shift of the depth habitat of *G. bulloides* toward the pycnocline, or decrease in the regional salinity - $\delta^{18}O_w$ slope at the LGM, would result in an overestimate of LGM cooling based on $\delta^{18}O_c$.

The offshore $\delta^{13}C$ gradient, measured in LGM *G. bulloides* shells, is compared with equilibrium calcite values ($\delta^{13}C_e$) predicted from water column $\delta^{13}C$ measurements on dissolved inorganic carbon in the same transect [*Ortiz et al.* 1996]. The watercolumn $\delta^{13}C_{DIC}$ are well correlated with dissolved nitrate, and thus we consider the isotopic data to be a good proxy for upper ocean nutrient gradients in this region. We emphasize gradients because absolute $\delta^{13}C$ values are affected by (1) the LGM $\delta^{13}C_{DIC}$ decrease relative to the Holocene ocean (about -0.4‰; *Curry and Crowley* [1987]), (2) the modern $\delta^{13}C_{DIC}$ decrease due to input of anthropogenic CO_2 into the upper ocean (-0.6±0.2‰ in this region [*Ortiz et al.* 1996]), and (3) the potential for $\delta^{13}C$ disequilibria in *G. bulloides*. For equation (3), we model the carbon isotopic disequilibrium in the $\delta^{13}C_e$ of *G. bulloides* as a function of calcification temperature, T_c, following *Ortiz et al.* [1996]:

$$\delta^{13}C_e = \delta^{13}C_s + 2.0^{(T_c-6.2)/10} \quad (3)$$

We use the LGM modern analog SST values derived from the foraminiferal faunas to estimate T_c.

Simulating Wind-Driven Upwelling

Upwelling, which injects nutrients into the upper ocean and thus supports biological productivity, is driven by the winds in two ways in this eastern boundary setting. First, along-shore winds from the north drive offshore Ekman transport. Coastal upwelling replaces the water moved offshore. Active coastal upwelling is limited to about 50 km offshore, mostly over the continental shelf, but its effects can extend farther offshore as coastal nutrients are advected seaward. Second, divergence of winds (wind stress curl) drives upwelling in the open ocean. In the northern hemisphere, positive (cyclonic) wind stress curl induces oceanic upwelling, whereas negative (anticyclonic) wind-stress curl results in downwelling. These mechanisms often reinforce each other but are not strictly linked. Changes in one mechanism can be decoupled from the other.

To isolate these two effects of coastal and open-ocean upwelling we calculated Ekman transport and wind stress curl using wind fields from the National Center for Atmospheric Research (NCAR) atmospheric regional climate model (RegCM). The version of the RegCM used here has 13 vertical levels and 60-km grid spacing over a 3000 x 3000 km domain centered at 38°N, 116°W (i.e., the corners of the model domain are NW=49.6°N, 137.3°W; NE=49.6°N, 94.6°W; SW=23.9°N, 130.1°W; SE=23.9°N, 101.9°W). Model wind fields from *Hostetler et al.* [1994] were sampled for 60 days to calculate offshore Ekman transport and wind stress curl. Perpetual January and July simulations were run using control (0 ka) and LGM (18 ka) boundary conditions derived from the coarse resolution COHMAP general circulation model (GCM) runs of *Kutzbach and Guetter* [1986].

The x and y components of wind stress ($\vec{\tau}$) are defined as:

$$\vec{\tau}_x = \rho C_d |\vec{u}| \vec{u}, \quad (4a)$$

and

$$\vec{\tau}_y = \rho C_d |\vec{v}| \vec{v}, \quad (4b)$$

where $\vec{\tau}_x$ and $\vec{\tau}_y$ are the wind stress components in dynes per square centimeter, and $|\vec{u}|\vec{u}$ and $|\vec{v}|\vec{v}$ are the products of the x or y component of wind speed and velocity [*Bakun and Nelson*, 1991]. The model wind field corresponds to a level about 40 m above sea level. Use of a constant logarithmic scaling factor to convert from 40 m to "standard" 10-m winds typically used for such calculations would decrease our wind stress estimates by 10-15% [*Stull*, 1988]. We hold air density (ρ) and the dimensionless drag coefficient (C_d) at 22 x 10^{-3} g cm^{-3} and 1.3 x 10^{-3} respectively [*Nelson*, 1977; *Bakun and Nelson*, 1991].

To calculate offshore Ekman transport, the along-shore coastal wind stress was obtained from the u and v components, then interpolated to 0.6° by 0.6° resolution, and divided by the Coriolis parameter, f.

Wind stress curl, the second wind variable we studied, is defined as:

$$\mathrm{curl}\vec{\tau} = \left(\frac{\partial \vec{\tau}^{(y)}}{\partial x} - \frac{\partial \vec{\tau}^{(x)}}{\partial y} \right). \quad (5)$$

We calculated wind stress curl on the model grid using a centered, finite difference scheme:

$$\mathrm{curl}\vec{\tau} = \left[\frac{\tau^y(i+1,j) - \tau^y(i-1,j)}{\Delta L_x} \right] - \left[\frac{\tau^x(i,j+1) - \tau^x(i,j-1)}{\Delta L_y} \right] \quad (6)$$

that approximates $\mathrm{curl}\vec{\tau}$ at grid location based on $\vec{\tau}_x$ and $\vec{\tau}_y$ at four neighboring grid points separated by distances ΔL_x and ΔL_y of 120 km [*Nelson*, 1977]. We did not employ the overlapping-grid method of *Bakun and Nelson* [1991] because unlike their irregularly spaced observations, our model wind fields are relatively smooth on a regularly spaced 60-km grid. Our wind stress curl estimates were interpolated to 0.6° by 0.6° resolution for graphic presentation using the nearest neighbor method, yielding resolution similar to the seasonal maps of *Bakun and Nelson* [1991].

Results

Comparison of Modern and Glacial Foraminiferal Faunas

Modern and LGM foraminiferal percentage data appear in Table 4, and the abundances of dominant species are illustrated in Figure 3. Left-coiling *N. pachyderma* (Figure 3a) and *G. bulloides* (Figure 3d) dominate the LGM fauna, accounting for >70% of the foraminifera at each site. This combination resembles the modern subpolar fauna of the Gulf of Alaska [*Sautter and Thunell*, 1989]. High percentages of these species occur in our LGM transect as far west as 130°W, some 650 km offshore. In contrast, left-coiling *N. pachyderma* and *G.*

bulloides are presently uncommon at 42°N, accounting for only about 10% of the fauna west of 128°W. Modern percentages rise to about 40% of the fauna at 126°W (300 km offshore).

Two more subpolar species, *Globigerina quinqueloba* and *Globigerinita glutinata*, were found at roughly equal percentages in both the modern and LGM data sets. Another, the deep-dwelling *Globorotalia scitula* [*Ortiz et al.* 1996] decreased in abundance in the LGM samples relative to the modern ones (Figure 3).

Transitional taxa, including *N. dutertrei*, decreased at LGM relative to present in the cores near the coast. Peak abundance of right-coiling *N. pachyderma* (30%) is similar in the modern and LGM assemblages (Figure 3h) but moved offshore during the LGM at the expense of modern subtropical species (*Orbulina universa* and *Globigerinoides ruber*) (Figure 3).

The LGM planktonic foraminiferal fauna at 42°N records expansion of subpolar conditions as far west as 130°W, trending to transitional waters offshore. These data are consistent with ice-age cooling across the entire transect. Similar to the modern distribution, the LGM fauna associated with cooler water occurred near the coast, while the warmer-water LGM fauna was found offshore. Some of the decrease in *O. universa* and *G. ruber* observed could reflect greater dissolution in LGM sediment samples than in modern sediment trap samples. If so, our results would overestimate the extent of ice-age cooling far offshore.

Modern Analog Sea Surface Temperatures

The modern analog SST estimates derived from the modern sediment trap faunas track atlas values at the coastal sites but overestimate SST at the site farthest offshore. The presence of *O. universa* and *G. ruber* drive the anomalous warmth in the offshore estimate [*Ortiz and Mix*, this issue]. These species are rare in N. Pacific core tops from midlatitudes, probably because they are highly sensitive to dissolution. Because the calibration data set is composed of partially dissolved core tops, this "no-analog" bias shows up in the well-preserved sediment trap samples. We expect that this bias is not a problem for the LGM samples.

The best modern analogs for the LGM California Current foraminifera are from core top sediments in the Gulf of Alaska, although some analog samples come from similar latitudes in the North Atlantic. The dissimilarity coefficients for each core were small (well below the empirical cutoff of 0.2), so the analogs are excellent (Table 5).

At the LGM, the annual average modern analog SST was 3.3°±1.5°C cooler than modern atlas SST at 42°N (Table 5, Figure 4). SST remained coolest near the coast and increased offshore. The LGM offshore thermal gradient was similar to today's (about 0.3°C / degree longitude). Given the 1.5°C error of the method, there was no statistically significant structure to the LGM - modern SST difference across the transect.

Oxygen Isotopes and Sea Surface Temperatures

The $\delta^{18}O$ of *G. bulloides* at the LGM was higher near the coast and lower offshore (Figure 5, Table 5). This gradient agrees with the sense of temperature gradients implied by the glacial fauna. Predictions of the oxygen isotopic composition of equilibrium calcite, $\delta^{18}O_c$, based on modern atlas SST and

Table 4. Modern and Glacial Planktonic Foraminiferal Faunas at 42°N

Location	Sample	% *O.un.*	% *G. ru.*	% *G. ca.*	% *G. fa.*	% *G. bu.*	% *T. hu.*	% *G. qu.*	% *N. pa.* L	% *N.Pa.* R	% *N. du.*	% *G. hx.*	% *G. in.*	% *G. cr.*	% *G. sc.*	% *G. gl.*	% *G. io.*	% *G. uv.*	% Other
6706-2	259-260	0.0	0.0	0.0	0.0	38.8	0.0	3.3	54.0	0.9	0.9	0.0	0.0	0.0	0.0	2.1	0.0	0.0	0.0
W8709A-13PC	275-276	0.0	0.0	0.0	0.0	35.4	0.0	4.2	51.5	3.3	0.0	0.0	0.0	0.0	0.4	5.3	0.0	0.0	0.0
W8809A-53GC	168-169	0.0	0.0	0.0	0.0	42.6	0.0	5.3	41.5	2.1	2.4	0.0	0.0	0.0	0.0	5.9	0.0	0.3	0.0
W8809A-21GC	140-141	0.0	0.0	0.0	0.0	23.7	0.0	7.4	54.4	3.5	1.1	0.0	0.0	0.0	1.1	8.5	0.0	0.0	0.4
W8709A-8PC	22-23	0.0	1.1	0.0	0.0	26.6	0.0	4.2	54.2	4.5	3.1	0.0	0.3	0.0	0.3	5.9	0.0	0.0	0.0
W8809A-29GC	156-157	0.0	0.0	0.0	0.0	43.3	0.0	9.2	38.3	3.3	0.8	0.0	0.0	0.0	0.8	4.2	0.0	0.0	0.0
W8809A-31GC	15-16	0.9	0.0	0.0	0.0	36.8	0.0	10.7	40.2	3.8	0.5	0.0	0.0	0.0	1.1	5.8	0.0	0.0	0.2
W8909A-57GC	22-23	0.6	0.0	0.0	0.0	45.2	0.0	4.7	37.0	3.6	1.8	0.0	0.0	0.0	0.0	7.1	0.0	0.0	0.0
W8709A-01BC	21-22	0.2	0.0	0.0	0.0	27.5	0.0	0.0	42.8	25.0	4.7	0.0	0.0	0.0	0.0	0.0	0.0	0.0	0.0
W8909A-48GC	17-18	0.6	0.0	0.0	0.0	32.4	0.0	1.0	35.2	26.3	3.8	0.0	0.0	0.0	0.0	0.0	0.0	0.0	0.6
NS sed. trap	annual	1.1	1.2	0.8	22.5	10.7	0.0	1.9	29.6	16.3	12.9	0.0	0.0	0.1	1.5	1.4	0.0	0.0	0.0
MD sed. trap	annual	9.0	3.5	0.2	5.4	16.6	0.0	6.5	7.8	23.9	11.9	0.0	0.5	0.0	8.2	6.5	0.0	0.0	0.0
Gyre sed. trap	annual	35.6	12.6	6.0	5.8	12.0	2.5	3.1	0.6	6.6	4.2	0.2	0.2	0.6	2.4	6.9	0.6	0.2	0.0

Species percentages may not add to 100 due to rounding.
O. un. = *Orbulina universa*; *G. ru.* = *Globigerinoides ruber*; *G. ca.* = *Globigerina calida*; *G. fa.* = *Globigerina falconensis*; *G. bu.* = *Globigerina bulloides*; *T. hu.* = *Turborotalita humilis*; *G. qu.* = *Globigerina quinqueloba*; *N. pa. L.* = *left-coiling Neogloboquadrina pachyderma*; *N. pa. R.* = *right-coiling N. pachyderma*; *N. du.* = *N. dutertrei*; *G. hx.* = *Globorotalia hexagona*; *G. in.* = *Globorotalia inflata*; *G. cr.* = *Globorotalia crassaformis*; *G. sc.* = *Globorotalia scitula*; *G. gl.* = *Globigerinita glutinata*; *G. io.* = *Globigerinita iota*; and *G. uv.* = *Globigerinita uvula*.

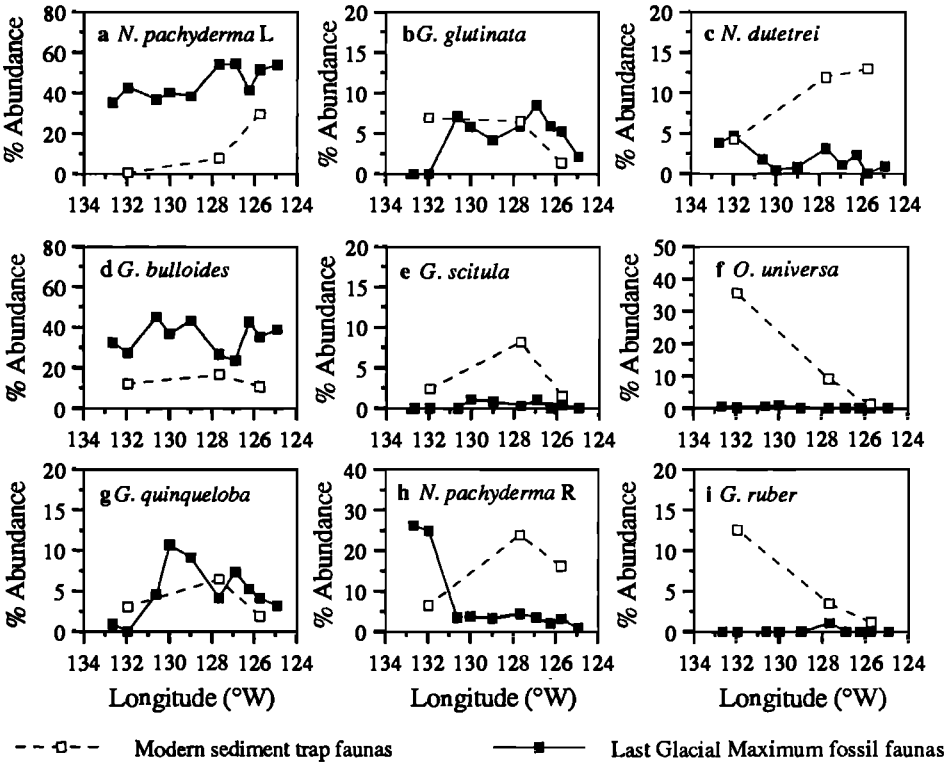

Figure 3. Planktic foraminifera species percentages across the transect at 42°N: (a) left coiling *N. pachyderma*, (b) *G. glutinata*, (c) *N. dutertrei*, (d) *G. bulloides*, (e) *G. scitula*, (f) *O. universa*, (g) *G. quinqueloba*, (h) right- coiling *N. pachyderma* and (i) *G. ruber*. Solid squares denote LGM horizon. Open squares denote modern sediment trap data based on flux-weighted averages of seasonal data reported by *Ortiz and Mix* [1992].

salinities, yield a zonal gradient in $\delta^{18}O_c$ of -0.09‰ $\delta^{18}O$ / degree longitude (r^2=0.79, n=10) at these sites. A similar gradient calculated from the LGM samples was -0.13‰ $\delta^{18}O$ / degree longitude (r^2=0.72, n=10). The offshore slope of the LGM $\delta^{18}O$ data suggests denser water (colder and/or saltier) near the coast relative to less dense water offshore, implying southward geostrophic flow as at present.

Assuming all of the observed gradients in $\delta^{18}O$ arose from temperature, the associated offshore thermal gradient would be 0.5° to 0.6 °C / degree longitude. This is about twice the temperature gradient at present, and twice that estimated from the LGM fauna (+0.3 °C / ° longitude). Possible explanations could be that (1) the LGM salinity gradient was steeper than the modern one, (2) the LGM salinity/$\delta^{18}O_w$ slope was steeper than

Table 5. LGM Modern Analog Method SST and LGM *G. bulloides* (300- 355 μm) Stable Isotope Measurements Across the Multitracers Transect

Core Name	Sample Depth, cm	Longitude, °W	Mean Dissimilarity	LGM SST[a]	Modern SST[b]	LGM- Present SST Change	$\delta^{18}O$, ‰ PDB	$\delta^{13}C$, ‰ PDB
6706-2	259-260	124.94	0.06	9.0	11.8	-2.8	2.79	-0.03
W8709A-13PC	275-276	125.75	0.07	10.0	12.3	-2.3	2.97	-0.27
W8809A-53GC	168-169	126.26	0.05	9.8	12.6	-2.8	3.16	0.20
W8809A-21GC	140-141	126.91	0.09	8.8	12.9	-4.1	2.70	0.07
W8709A-08PC	22-23	127.68	0.05	9.3	13.3	-4.0	2.81	-0.06
W8809A-29GC	156-157	129.00	0.06	9.8	13.8	-4.0	2.28	0.07
W8809A-31GC	15-16	130.01	0.10	10.6	14.1	-3.5	2.67	-0.09
W8909A-57GC	22-23	130.62	0.05	9.8	14.2	-4.4	2.52	0.37
W8709A-01BC	21-22	131.96	0.09	11.8	14.4	-2.6	2.19	0.82
W8909A-48GC	17-18	132.67	0.09	11.8	14.5	-2.7	1.82	0.87

[a]Based on foraminiferal faunas using the modern analog method, associated errors are ±1.5 °C.
[b]Interpolated to core locations from *Levitus* [1982].

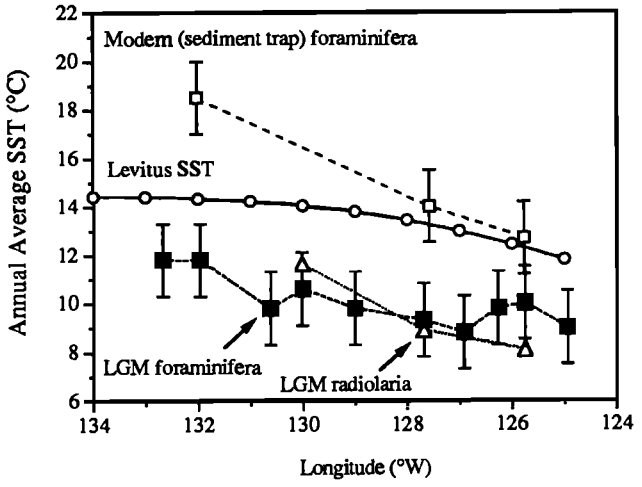

Figure 4. Temperature gradients across the transect. Modern thermal gradient (open circles) is from *Levitus* [1982]. Modern analog SST estimates based on the sediment trap faunas (open squares) are from *Ortiz and Mix* [this issue]. Solid squares denote modern analog SST estimates based on glacial-age foraminiferal fauna . Imbrie-Kipp transfer function SST estimates are based on LGM radiolarian faunas. Radiolarian results from ~126°W and ~128°W are from *Sabin and Pisias* [1996]. Radiolarian SST estimate at ~130°W is from this study. Error bars are ±1.5°C for both foraminiferal and radiolarian SST estimates.

the modern slope, or (3) *G. bulloides* lived deeper in the water column nearer the coast during the LGM.

The $\delta^{18}O$ of LGM *G. bulloides* is higher by ~3‰ than modern $\delta^{18}O_c$ predicted for the sea surface (Figure 5). After accounting for a 1.3‰ ice volume effect on mean ocean $\delta^{18}O_w$, we can estimate an upper limit for the LGM temperature change across the transect, assuming the slope of the regional salinity/$\delta^{18}O_w$ relationship was unchanged, and *G. bulloides* calcified in the mixed layer (its present habitat at these sites as recorded by MOCNESS plankton tows). This estimate suggests the magnitude of the LGM cooling at these sites could have been 4°- 6°C at most. For comparison, we have plotted the foraminiferal modern analog LGM SST estimates as equivalent $\delta^{18}O_c$ predictions using the same assumptions (Figure 5).

A 4°-6°C cooling based on the oxygen isotope data is at the upper statistical limit of the 3.3°±1.5°C cooling estimated by the modern analog faunal method. However, it is likely some of this apparent 4°-6°C cooling reflects local increases in salinity driven by stronger ice-age upwelling, or a change of the depth habitat of *G. bulloides*. For example, the deviations between the modern analog paleotemperatures expressed as $\delta^{18}O_c$ and the *G. bulloides* $\delta^{18}O$ measurements can be minimized in a least squares sense, yielding a residual of 0.09‰ (approximately our $\delta^{18}O$ machine precision) using a $\delta^{18}O$ offset of -0.75±0.05‰. This offset is smaller than the 1‰ offset relative to surface waters attributed to modern *G. bulloides* in the Gulf of Alaska due to a depth habitat near 100 m [*Zahn et al.* 1991a]. Thus, while *G. bulloides* $\delta^{18}O$ helps to constrain the zonal thermal gradient it does not provide a unique measure of the absolute temperature change.

Carbon Isotopes and Nutrient Gradients

In the absence of active upwelling, modern surface waters (offset to the LGM mean) yield $\delta^{13}C_c$ predictions near 2.5‰ with small variation across the transect (Figure 6). Active upwelling brings nutrient-rich waters from around 70 m depth to the surface (Figure 6). This reduces surface $\delta^{13}C_c$ to values near those at 100 m at the same site. The modern $\delta^{13}C_c$ at 100m increases offshore by about 1‰. This shift reflects shoaling of the nutricline in response to southward geostrophic flow and local wind forcing.

The $\delta^{13}C$ of LGM *G. bulloides* range from -0.27‰ near the coast to 0.87‰ near 132.5°W (Figure 6, Table 5). After disequilibrium effects are estimated and removed (equation 3), the mean $\delta^{13}C$ of *G. bulloides* approximates water column $\delta^{13}C_c$ derived from measurements of water column $\delta^{13}C_{DIC}$ corrected for the anthropogenic $\delta^{13}C_{DIC}$ decrease and the mean ocean's glacial-interglacial $\delta^{13}C_{DIC}$ shift. The offshore gradient in $\delta^{13}C$ remains, suggesting large offshore nutrient gradients as at present. Westward translation of the LGM $\delta^{13}C_c$ gradient relative to the present gradient suggests westward translation of the associated nutrient gradients, perhaps coupled to an increase in net upwelling as far west as 130°W.

Shell Accumulation Rates and Foraminiferal Productivity

The accumulation rates of left-coiling *N. pachyderma* and *G. bulloides* shells near 126°W are much greater at the LGM than in the modern sediment traps (Figure 7). This cannot be an artifact of dissolution, because the LGM sediment samples are

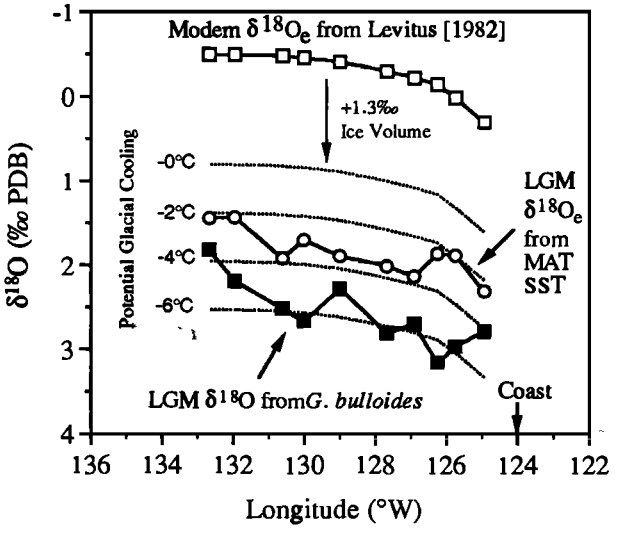

Figure 5. Oxygen isotopic composition ($\delta^{18}O$) of *G. bulloides* from LGM sediments across the Multitracers transect. Shown for comparison are equilibrium calcite $\delta^{18}O$ for modern waters (open squares). The *G. bulloides* data are consistent with a 4°-6°C cooling assuming (1) an ice volume effect of +1.3‰, (2) the modern S- $\delta^{18}O$ slope of +0.41 also applies during the glacial, and (3) a mixed layer depth habitat. The foraminiferal modern analog SST estimates (open circles) suggest a 2°-4°C cooling.

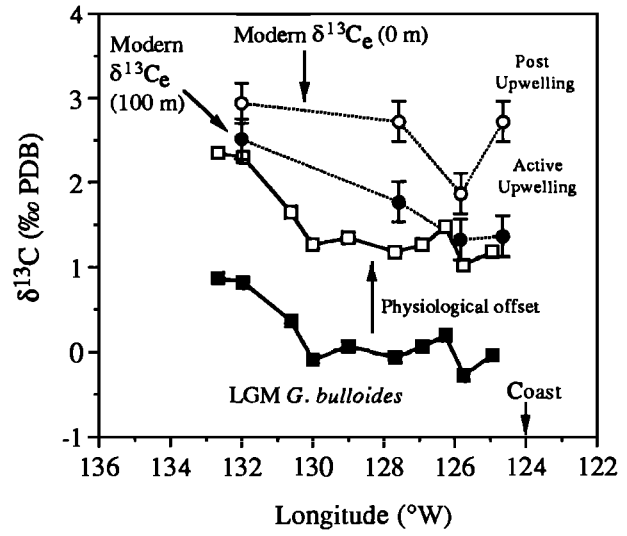

Figure 6. Carbon isotopic composition ($\delta^{13}C$) of *G. bulloides* from glacial sediments across the 42°N transect. The magnitude of the carbon isotopic disequilibrium (physiological offset, $\Delta\delta^{13}C_{e-s}$) in *G. bulloides* is estimated using equation 3. Modern $\delta^{13}C_e$ values at 42°N based on measurements from *Ortiz et al.* [1996] are plotted for reference after being offset for the glacial $\delta^{13}C_{DIC}$ shift of -0.4‰ and the anthropogenic shift of -0.6‰.

more dissolved than the modern sediment trap samples. Given potential errors in sediment accumulation rates associated with timescale uncertainties, we hesitate to interpret structure in the decreasing offshore accumulation rates. Given the consistency of the result, however, the net increase relative to modern fluxes appears robust. Because these species are heterotrophic, they are sensitive to food supply and thus to productivity (*Ortiz et al.* 1996). We interpret the higher LGM accumulation rates of these species as due to higher productivity of the heterotropic foraminifera. This is consistent with the carbon isotopic evidence for westward expansion of nutrient supplies noted above.

Ekman Transport and Coastal Upwelling

The seasonal offshore Ekman transport simulated by the RegCM for modern boundary conditions captures the basic structure and magnitude of the coastal upwelling seasonal cycle in the California Current (Figure 8). Consistent with observations [*Huyer*, 1983], north of 40°N, coastal upwelling is seasonal, strong in July but absent (or downwelling) in January. Between 30°N, and 40°N, coastal upwelling persists throughout the year, but is strongest in summer. South of 30°N both observations and the model record roughly constant coastal upwelling throughout the year.

North of 45°N, model- simulated offshore Ekman transport exceeds observed values for both seasons. This feature probably reflects edge effects at the northern boundary of the model domain. Peaks in observed offshore transport between 35°N and 40°N are displaced southward by the model by 1°-2° latitude. This most likely reflects difficulty defining coastline shape precisely in the gridded model.

Simulated offshore Ekman transport at the LGM was lower in both seasons than it is at present (Figure 8). North of 42°N the model predicts coastal downwelling in both seasons. Major reductions in summer upwelling occur north of 40°N, and winter downwelling occurs as far south as 33°N. South of 33°N, predicted changes in coastal upwelling are relatively small, probably within the range of model uncertainties. The overall

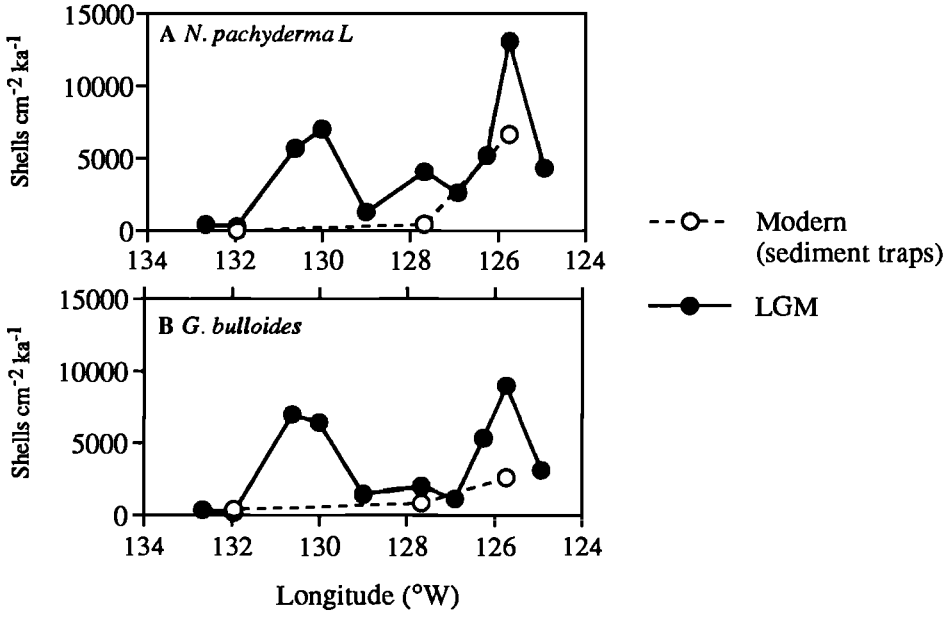

Figure 7. Shell accumulation rates for (a) left-coiling *N. pachyderma* and (b) *G. bulloides*, two heterotrophic planktonic foraminifera. Modern rates are derived from annually average sediment trap flux at the three sediment-trap mooring sites. LGM shell accumulations are from the 10 cores across the 42°N transect.

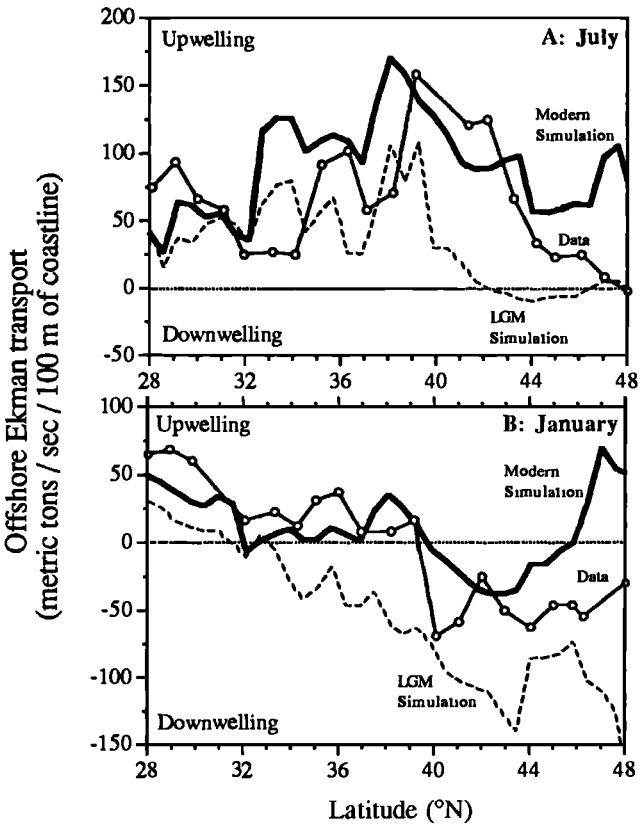

Figure 8. Observed and simulated offshore Ekman transport for the California Current. (a) Modern observations for July compared with modern and LGM July simulations. (b) Modern observations for January compared with modern are based on winds from the NCAR RegCM runs of *Hostetler et al.* [1994].

reduction in coastal upwelling at the LGM is associated with southward translation of atmospheric pressure systems and associated winds, which is driven in the model by large northern hemisphere ice sheets and lower sea surface temperatures.

Wind Stress Curl and Open-Ocean Upwelling

Bakun and Nelson [1991] report modern seasonal variations in wind stress curl over the California Current. In winter, west of 126°W along our 42°N transect, curl is negative, yielding downwelling in the interior of the subtropical gyre. In summer, positive curl drives strong upwelling east of 128°W. South of 40°N, positive curl near the coast persists throughout the year, and thus offshore upwelling reinforces year-round coastal upwelling in this area. The RegCM simulations of wind stress curl for modern January (Figure 9a) and July (Figure 9d) capture these basic features. In January, simulated curl is negative offshore, consistent with observations. Positive curl persists near the coast in both seasonal simulations, especially south of about 40°N.

The model simulations are not perfect, however. North of 47°N, simulated curl is always positive, unlike observations. This is probably an edge effect near the northern limit of the RegCM domain. Similarly, edge effects of positive curl simulated along the western boundary south of 32°N, and negative curl simulated along the southern boundary, are unrealistic. The modern July simulation also indicates local zones of intense convergence (negative curl) near the upwelling front at 38°N and 32°N. These features are not present in the maps of *Bakun and Nelson* [1991]. Given these apparent weaknesses in the model simulations, we only interpret broad features, and rely on difference maps between modern and ice-age conditions. The hope is that model biases common in both runs would tend to cancel, minimizing the net bias in the difference maps.

The LGM wind stress curl simulations suggest enhanced positive curl in offshore regions for both the January and July simulations (Figures 9b and 9e). LGM-minus-modern difference maps confirm that ice-age curl was more positive offshore in both January and July. In the LGM January simulation, curl decreased near the coast north of 33°N. Thus, on an annual average basis, the model simulations suggest a net westward translation of curl-driven upwelling offshore between 30°N and 42°N during the LGM, relative to conditions at present.

Discussion

The Glacial Temperature Decrease

Our results suggest that the mean annual SST at 42°N during the LGM was 3.3°±1.5°C cooler than present. This temperature estimate is consistent with the radiolarian faunal temperature estimates of *Moore* [1973] and *Moore et al.* [1980] in three cores near our locations. Similarly, *Prahl et al.* [1995] compared temperature estimates based on U^k_{37} and radiolarian faunal estimates in one core studied here (W8709A-8PC) and inferred an LGM temperature decrease of 4.0°±1.5°C, similar to our estimate.

The agreement between these methods is somewhat surprising. Measurements of the U^k_{37} index in sediment traps at the same sites used here yielded an annual temperature of 10.6°±1.1°C with no significant offshore gradient [*Prahl et al.* 1993]. This estimate is significantly cooler than the 12°-15°C annual mean SST at these sites. Prymnesiophyte algae which generate the alkenone signal bloom in the spring and summer and reside within the thermocline, rather than at the sea surface [*Prahl et al.* 1993]. In contrast, the radiolarian transfer function generates temperatures based on the calibration of Holocene faunas against mean annual sea surface temperature. According to *Prahl et al.* [1995], these two seemingly different methods produce similar temperature estimates because in the North Pacific, mean annual SST over the range 0°-15°C is equivalent to the summer temperature at the pycnocline.

Sabin and Pisias [1996] used the same radiolarian transfer function as *Prahl et al.* [1995] in a meridional transect from 35° to 55°N. Their transect included two cores used here (W8709A-8PC and W8709A-13PC). We supplement the two published LGM radiolarian temperature estimates at 42°N with one from W8809A-31GC (radiolarian taxonomy courtesy of M. Webber, Oregon State University). The resulting radiolarian SST estimates yield LGM cooling of 4.2°±1.5°C, 4.4°±1.5°C, and 2.4°±1.5°C in the three sites relative to modern atlas values, indistinguishable from the foraminiferal-based estimate of 3.3°±1.5 °C cooling in this region (Figure 4).

The 3°-4°C cooling we estimate was roughly constant across the entire east-west transect. Our estimate is smaller than the

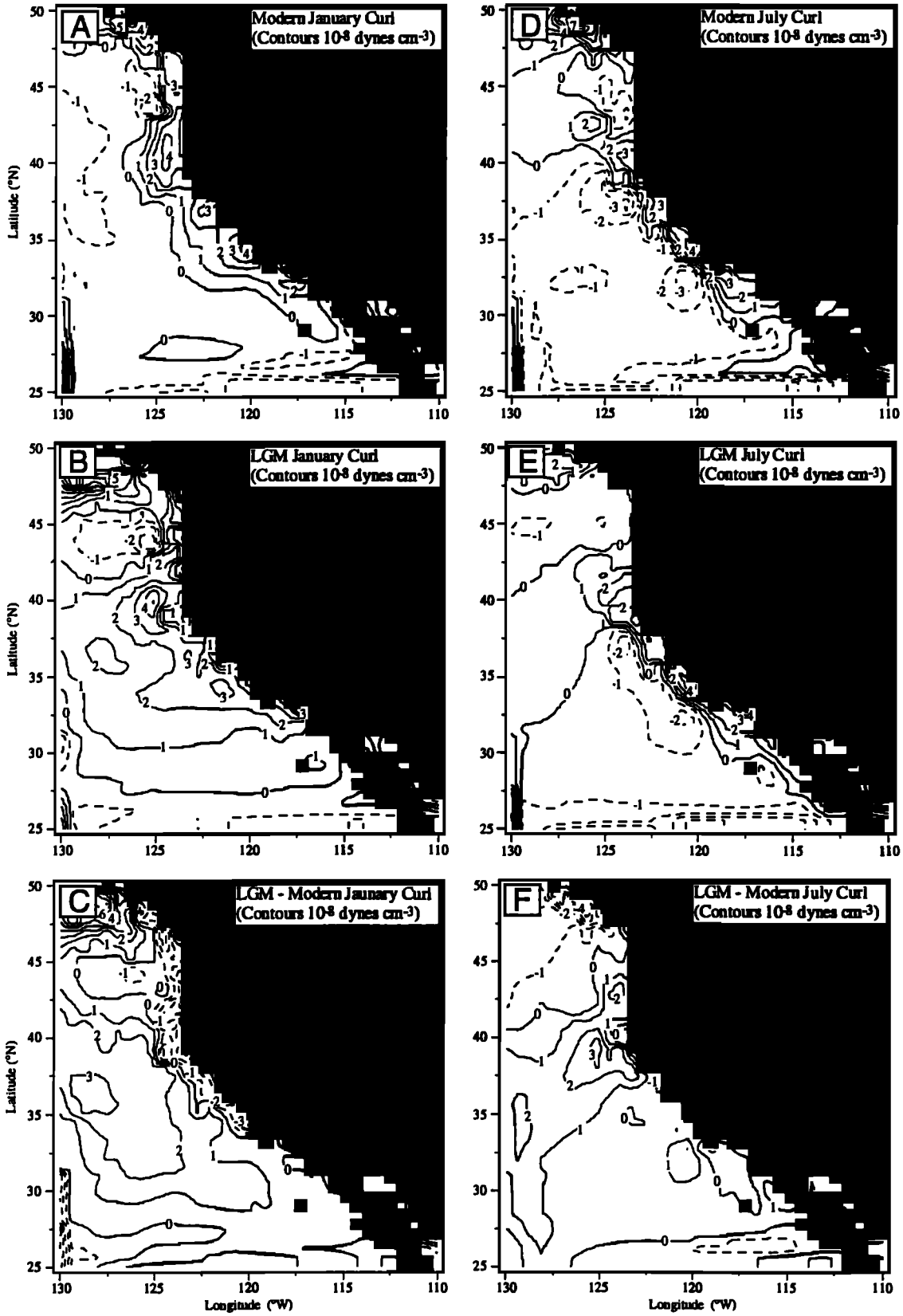

Figure 9. Simulated wind stress curl for the California Current region. Results are from (a) modern January, (b) glacial January, (c) glacial January-modern January, (d) modern July, (e) glacial July, and (f) glacial July-modern July. Contours are in 10^{-8} dynes cm^{-3}. Cyclonic wind stress curl (positive values, solid contours) drives oceanic upwelling. Anticyclonic wind stress curl (negative values, dashed contours) drives oceanic downwelling. The calculations are based on winds from the NCAR RegCM runs of *Hostetler et al.* [1994].

5°-10°C cooling suggested by *Mortyn et al.* [1996] from $\delta^{18}O$ of *G. bulloides* in the Southern California Borderland sediments, but larger than the 1.5°C cooling based on the U^{k}_{37} temperature index in ocean drilling program (ODP) Site 893 from the Santa Barbara Basin [*Herbert et al.* 1995]. These differences may in part reflect regional temperature variations, although *Mortyn et al.* [1996] did not attempt to constrain the effect of upwelling-related salinity variations on $\delta^{18}O$, which would likely reduce the amplitude of their inferred cooling.

Zonal Thermal Gradients and Southward Flow

At 42°N, LGM temperatures remained coolest near the coast and increased offshore. This pattern is similar to the modern zonal thermal gradient at this latitude and suggests that a southward flowing California Current was still present during the LGM. The steeper offshore $\delta^{18}O$ gradient relative to the modern water column $\delta^{18}O_w$ gradient at 42°N may suggest a stronger density gradient, and if so, geostrophy would require enhanced southward advection. However, this possibility should be viewed with caution due to uncertainties in the slope of the LGM S-$\delta^{18}O$ relationship and foraminiferal depth habitats.

Southward flow at 42°N requires that the LGM polar front remained north of our sites. Had the Polar front shifted south of our locations, local wind forcing would have been more heavily influenced by the cyclonic Aleutian low. In response, a poleward flowing eastern boundary current of the subarctic gyre would have replaced the California Current over our sites. Under such conditions, one would expect to see cold, nutrient-enriched water throughout the transect, with a zonal thermal gradient reversed from that observed (i.e. warmer temperatures near the coast with a gradual offshore cooling). This pattern, which is similar to the modern wintertime regime at 42°N, would be associated with offshore oceanic upwelling in the LGM subarctic gyre.

Enhanced Glacial Nutrient Content

We observed a >1‰ $\delta^{13}C$ enrichment in LGM *G. bulloides* shells offshore relative to those near the coast (Figure 6). This enrichment does not appear to be related to the organism's physiological carbon isotopic disequilibrium as predicted for temperature effects [*Ortiz et al.* 1996]. Paleoceanographic factors that could cause the enrichment include variations in air-sea equilibration state, nutrient content, or some combination of both effects. Local equilibration with the atmosphere seldom reaches completion in surface waters due to differences in the time of contact with the atmosphere (order of months) relative to the time required for isotopic equilibration (order of years to decades) and competing biological carbon transports. If $\delta^{13}C_{DIC}$ were fully equilibrated with the atmosphere (holding other effects constant), it would follow a slope near -0.14‰ $\delta^{13}C_{DIC}$ / °C so that the $\delta^{13}C_{DIC}$ in colder water would be higher than in warmer water [*Kroopnick*, 1974]. In this case, we would expect *G. bulloides* shells closer to the coast to record $\delta^{13}C$ values +0.4‰ higher than those offshore. This is not the case. A better explanation of increasing $\delta^{13}C$ offshore is that surface waters rich in nutrients are low in $\delta^{13}C_{DIC}$, whereas those depleted in nutrients are high in $\delta^{13}C_{DIC}$. The LGM offshore gradient of $\delta^{13}C$ in *G. bulloides* thus implies higher nutrient content near the coast and lower nutrient content offshore.

The LGM $\delta^{13}C$ gradient in *G. bulloides* across 42°N is steeper than the modern water column gradient at the sea surface. It is similar to the modern $\delta^{13}C_c$ gradient at 100 m (Figure 6). The offshore subsurface enrichment trend in the modern ocean begins east of 128°W. In the LGM samples, high $\delta^{13}C$ values are not encountered east of 130°W. If *G. bulloides* occupied a surface habitat, LGM surface waters were greatly enriched in nutrients relative to modern ones across the entire transect. If *G. bulloides* occupied a depth habitat closer to 100 m (consistent with its apparent modern Gulf of Alaska habitat), then offshore waters were enriched in nutrients down to ~100m, and coastal waters carried roughly the same nutrient content as modern waters. In either case, LGM nutrients in offshore regions of the California Current at 42°N were most likely slightly to greatly enhanced relative to their modern values. Variations in LGM wind forcing could cause such a nutrient change by (1) enhancing coastal upwelling due to greater offshore Ekman transport, (2) enhancing oceanic upwelling resulting from greater wind stress curl, or (3) enhancing southward flow due to stronger basin scale wind stress curl.

We discount the first mechanism because the RegCM results suggest that coastal upwelling north of 35°N decreased in the California Current during the LGM (Figure 8), a result which is consistent with lower accumulation rates of coastal diatoms [*Sancetta et al.* 1992] and marine organic carbon [*Lyle et al.* 1992]. RegCM simulations support the second mechanism, enhanced LGM wind-stress curl in the California Current relative to modern conditions (Figure 9). This implies that enhanced oceanic upwelling supplied nutrients from below to increase the nutrient content of offshore LGM waters, decrease their $\delta^{13}C$ composition, and indirectly produce the observed increase in offshore accumulation rates of heterotrophic foraminiferal shells by increasing prey density.

The third potential mechanism for increasing the nutrient content of the LGM California Current is enhanced southward flow. As noted previously, the offshore gradient of LGM $\delta^{18}O$ is consistent with enhanced southward advection during the LGM. The coarse resolution atmospheric GCM results *of Kutzbach and Guetter* [1986] suggest that North Pacific winds were stronger and displaced southward at the LGM. These changes could increase the proportion of cold, nutrient-rich water flowing from the LGM North Pacific Current, into the equatorward LGM California Current, as opposed to the poleward LGM Alaskan Current. This would shift the character of the LGM California Current toward more subarctic conditions and result in the upward tilting of isopycnals, a geostrophic readjustment to enhanced southward flow. A similar concept explains years with anomalous subarctic zooplankton biomass in the modern California Current [Chelton, 1982; Chelton and Davis, 1982; Chelton *et al.* 1982].

The net results of both the second and third mechanisms would be to cool the surface waters of the LGM California Current and increase its nutrient content. These changes would in turn produce waters with lower $\delta^{13}C$ values farther offshore and increase the offshore shell accumulation rates of heterotrophic foraminifera. As a result, we cannot definitively

distinguish between these mechanisms. Mechanisms 2 and 3 are not entirely independent, however, because large-scale variations in wind stress curl provide the forcing for the Sverdrup balance as well as for local open-ocean upwelling [*Chelton*, 1981, 1982].

Community Ecology of the Glacial California Current

The foraminiferal fauna of the LGM California Current at 42°N is similar to that of the modern Gulf of Alaska. Does the ecologic shift recorded by the foraminifera reflect the plankton community as a whole? Perhaps.

Marine organic carbon accumulation rates in some of the sites studied here were lower during the LGM than at present, suggesting lower carbon export [*Lyle et al.* 1992]. Accumulation rates of *Chaetoceros* spores, diatom indicators of the modern coastal upwelling ecosystem, were also low during the LGM [*Sancetta et al.* 1992]. Ice-age pollen assemblages were dominated by pine and mountain hemlock, in contrast to the modern assemblage of oak, redwood, and alder [*Sancetta et al.* 1992]. Loss of redwood and alder at the LGM suggests a reduced moisture supply due to loss of summer coastal fog. Fog is generated by relatively warm atmosphere over colder (upwelled) oceanic waters. These results all suggest lower coastal upwelling during the LGM.

Reduction of coastal upwelling, coupled with our evidence for higher nutrient content and foraminiferal shell fluxes along most of the 42°N transect during the LGM, suggest an ecosystem similar to that of the modern Gulf of Alaska. The modern California Current is a high-nutrient, high-chlorophyll, high-export ecosystem. The dominant primary producers in this environment are large diatoms [*Hood et al.* 1990]. These diatoms, and the macrozooplankton that graze on them, export a relatively large fraction of the total biological productivity as fecal pellets and sinking particles. In contrast, the Gulf of Alaska is a high-nutrient, low-chlorophyll, low-export system. An active microbial loop, composed of a variety of small autotrophs and heterotrophs, makes recycling more efficient here than in the California Current [*Miller et al.* 1991]. In such systems, a smaller fraction of organic matter sinks to the seafloor.

The decrease in export productivity of the LGM California Current at 42°N is ultimately linked to changes in the physical environment. However, these physical changes did not simply cause the biological interactions of the modern oceanic community to run more slowly. Rather, the physical changes appear to have resulted in the replacement of the high-export flux, modern coastal upwelling community with a low-export flux, subarctic, open-ocean upwelling community.

Conclusions

Foraminiferal species and isotopic data from 10 sediment cores suggest the magnitude of the LGM temperature decrease across the California Current at 42°N during the LGM was 3.3° ±1.5°C. The cooling was roughly constant across the entire transect. Temperatures remained coolest near the coast and increased offshore, similar to the modern annual average zonal thermal gradient. These findings suggest that the equatorward flowing California Current was still present at 42°N during the LGM, and that the polar front must have remained north of this latitude band.

Cooling was likely a response to stronger open-ocean upwelling and southward advection driven by higher wind stress curl. Coastal upwelling decreased at 42°N during the LGM.

LGM waters of the California Current were relatively high in nutrients offshore (based on carbon isotope data) and low in biomass due to more intense grazing by microorganisms (based on reduced organic carbon accumulation rates and increases in heterotrophic plankton). This suggests that during the LGM the plankton community of the northern California Current was similar to the modern plankton community of the Gulf of Alaska.

Acknowledgments. We thank the captain and crew of R/V *Wecoma*. J. Gardner (USGS) kindly provided unpublished ^{14}C dates. M. Webber and L. Welling assisted with the radiolarian data. Comments from N. Pisias, P. Wheeler, M. Abbott, L. Welling, and reviews from J. Gardner, D. Anderson, and an anonymous reviewer were helpful. Funding was from a NASA Graduate student fellowship and from NSF. Curation of materials at OSU was funded by NSF. This is Lamont-Doherty Earth Observatory contribution 5599.

References

Bakun, A., and C.S. Nelson, The seasonal cycle of wind-stress curl in subtropical eastern boundary current regions, *J. Phys. Oceanogr., 21*, 1815-1834, 1991.

Bard, E., M. Arnold, and B. Hamelin, Present status of the radiocarbon calibration for the Late Pleistocene (IPC4 abstracts and supplementary materials). *GEOMAR Report 15*, 52-53, 1992.

Bard, E., M. Arnold, R.G. Fairbanks, and B. Hamlin, ^{230}Th-^{234}U and ^{14}C ages obtained by mass spectrometry on corals, *Radiocarbon, 35*, 191-199, 1993.

Barnard, A.H., Seasonal variability of zooplankton off the California coast: A box model approach, M.A. thesis, 91 pp., Oregon State Univ., Corvallis, 1994.

Bé, A.W.H., An ecological, zoogeographic, and taxonomic review of recent planktonic foraminifera, in *Oceanic Micropaleontology*, vol. 1, edited by A.T.S. Ramsey, pp. 1-100, Academic, San Diego, Calif., 1977.

Chelton, D.B., Interannual variability of the California Current - Physical factors, Calif. Coop. *Fish. Invest. Rep. XXII*, 34-48, 1981.

Chelton, D.B., Large-scale response of the California Current to forcing by the wind stress curl, *Calif. Coop. Fish. Rep. XXIII*, 130-148, 1982.

Chelton, D.B., and R.E. Davis, Monthly mean sea-level variability along the west coast of North America, *J. Phys. Oceanogr., 12*, 757-784, 1982.

Chelton, D.B., P.A. Bemal, and J.A. McGowan, Large-scale interannual physical and biological interaction in the California Current, *J. Marine Res., 40*, 1095-1125, 1982.

Craig, H., and L.I. Gordon, Deuterium and oxygen-18 variations in the ocean and marine atmosphere, in Stable Isotopes in Oceanographic Studies and Paleotemperatures,*Third SPOLETO Conference on Nuclear Geology*, edited by E.Tiongiorini, pp. 9-130, Cons. Naz. Ric. Lab. Geol. Nucl., Pisa, Italy, 1965.

Curry, W.B., and T.J. Crowley, The $\delta^{13}C$ of equatorial Atlantic surface waters: Implications for Ice Age pCO_2 levels, *Paleoceanography, 2*, 489-517, 1987.

Epstein, S., R. Buchsbaum, H.A. Lowenstam, and H.C. Urey, Revised carbonate- water isotopic temperature scale,. *Geol. Soc. Am. Bull., 64*, 1315-1326, 1953.

Fairbanks, R.G., A 17,000-year glacio-eustatic sea level record: Influence of glacial melting rates on the Younger Dryas event and deep-ocean circulation, *Nature, 342*, 637-642, 1989.

Faure, G., *Principles of Isotope Geology*, 2nd ed., 464 pp., John Wiley, New York, 1977.

Gardner, J., W. Dean, and P. Dartnell, Biogenic sedimentation beneath the California Current System for the past 30 ka and itspaleoceanographic significance, *Paleoceanography*, this issue.

Hemleben, C., M. Spindler, and O.R. Anderson (Eds.), *Modern Planktonic Foraminifera*, 363 pp., Springer-Verlag, New York, 1988.

Herbert, T.D., M. Yasuda, and C. Burnett, Glacial-interglacial sea-surface temperature record inferred from alkenone unsaturation indices, Site 893, Santa Barbara Basin, Proc. *Ocean Drill Program, Sci. Results, 146*, 257-264, 1995.

Hood, R.R., M.R. Abbott, A. Huyer, and P.M. Kosro, Surface patterns in temperature, flow, phytoplankton biomass, and species composition in the coastal transition zone off northern California, *J. Geophys. Res, 95*, 18081-18094, 1990.

Hostetler, S.W., F. Giorgi, G.T. Bates, and P.J. Bartlein, Lake-atmosphere feedbacks associated with paleolakes Bonneville and Lahontan, *Science, 263*, 665-668, 1994.

Huyer, A., Coastal upwelling in the California Current system, *Prog. Oceanogr., 12*, 1434-1450, 1983.

Karlin, R., M. Lyle, and R. Zahn, Carbonate variations in the northeast Pacific during the late Quaternary, *Paleoceanography, 7*, 43-62, 1992.

Kipp, N.G., New transfer function for estimating past sea-surface conditions from sea- bed distributions of planktonic foraminiferal assemblages in the North Atlantic, in Investigations of late quaternary paleoceanography and paleontology, edited by K.K. Turekian, Memo,*Geol. Soc., Am., 145*, 3-41, 1976.

Kroopnick, P., Correlations between ^{13}C and ΣCO_2 in surface waters and atmospheric CO_2, *Earth and Planet. Sci. Lett. 22*, 397-403, 1974.

Kutzbach, J., and P.J. Guetter, The influence of changing orbital parameters and surface boundary conditions on climatic simulations for the past 18,000 years, *J. Atmos. Sci., 16*, 1726-1759, 1986.

Levitus, S., Climatological atlas of the world ocean, *NOAA Prof. Pap. 13*, 173 pp., U.S. Govt. Print. Off., Washington, D.C., 1982.

Lyle, M., R. Zahn, F. Prahl, J. Dymond, R. Collier, N. Pisias, and E. Suess, Paleoproductivity and carbon burial across the California Current: The Multitracers transect, 42°N, *Paleoceanography, 7*, 251-272, 1992.

Miles, G.A., Living planktonic foraminifera in the northeast Pacific Ocean, M.A. thesis, 131pp., Univ. of Oregon, Eugene, 1973.

Miller, C.B., B.W. Frost, B. Booth, P.A. Wheeler, M.R. Landry, and N. Welschmeyer, Ecological processes in the subarctic Pacific: Iron limitation cannot be the whole story, *Oceanography, 4*, 71-78, 1991.

Mix, A.C., The oxygen-isotope record of glaciation, in *North America and Adjacent Oceans During the Last Deglaciation*, The Geology of North America, *vol. K-3*, edited by W.F. Ruddiman, and H.E. Wright Jr., pp. 111-135, *Geol. Soc. of Am.*, Boulder, Colo., 1987.

Moore, T.C., Late Pleistocene-Holocene oceanographic changes in the northeastern Pacific, *Quat. Res., 3*, 229-266, 1973.

Moore, T.C., L.H. Burkle, K. Geitznauer, B. Luz, A. Molina-Cruz, J.H. Robertson, H. Sachs, C. Sancetta, J. Thiede, P. Thompson, and C. Wenkam, The reconstruction of sea surface temperatures in the Pacific Ocean 18,000 B.P., *Marine Micropaleontol., 5*, 215-247, 1980.

Mortyn, P.G., R.C. Thunell, D. Anderson, L.D. Stott, and J. Le, Sea surface temperature changes in the southern California Borderlands during the last glacial-interglacial cycle, *Paleoceanography, 11*, 415-430, 1996.

Nelson, C.S., Wind stress and wind-stress curl over the California Current, NOAA Tech. Rep. NMFS SSRF-714, U.S. Dept. of Commerce, 87 pp., 1977.

Ortiz, J.D., Planktic foraminifers of the California Current at 42°N: Last Glacial Maximum and Present, Unpublished Ph.D. Dissertation, Oregon State University, 219 pp., 1995.

Ortiz, J.D., and A.C. Mix, The spatial distribution and seasonal succession of planktonic foraminifera in the California Current off Oregon, September 1987-1988, in *Upwelling ssystems: evolution since the early Miocene*, edited by C.P. Summerhayes, W.L. Prell, and K.C. Emeis, *Geol. Soc. Spec. Publ. 64*, London, 197-213, 1992.

Ortiz, J.D., and A.C. Mix, Comparison of Imbrie-Kipp transfer function and modern analogtemperature estimates using sediment trap and core top foraminiferal faunas, *Paleoceanography*, this issue.

Ortiz, J.D., A.C. Mix, and R.W. Collier, Environmental control of living symbiotic and asymbiotic planktonic foraminifera in the California Current, *Paleoceanography, 10*, 987-1009, 1995

Ortiz, J.D., A. C. Mix, W. Rugh, J. M. Watkins, and R. W. Collier, Deep-dwelling planktonic foraminifera of the NE Pacific record intermediate water properties, *Geochim. Cosmochim. Acta, 22*,4509-4523, 1996.

Östlund, H.G., H. Craig, W.S. Broecker, and D. Spencer (Eds.), *GEOSECS Atlantic, Pacific, and Indian Ocean Expeditions, Shorebased Data and Graphics, GEOSECS Atlas Ser.*, vol. 7, 200 pp., U.S. Gov. Print. Off., Washington, D.C., 1987.

Parker, F., Planktonic foraminiferal species in Pacific sediments, *Micropaleontology, 8*, 219-254, 1962.

Prahl, F.G, R.B. Collier, J. Dymond, M. Lyle, and M.A. Sparrow, A biomarker perspective on prymnesiophyte productivity in the northeast Pacific Ocean, *Deep Sea Res. Part 1, 40*, 2061-2076, 1993.

Prahl, F.G., N.G. Pisias, A.L. Sabin and M. Sparrow, Assessment of sea surface temperature at 42°N in the California Current System over the last 30,000 years, *Paleoceanography, 10*, 763-773, 1995.

Sabin, A.L., and N.G. Pisias, Sea surface temperature change in the northeast Pacific Ocean for the past 20,000 years and its relationship to climatic change in the Pacific Northwest of North America, *Quat. Res, 46*, 48-61, 1996.

Sancetta, C., M. Lyle, L. Heusser, R. Zahn, and J.P. Bradbury, Late-Glacial to Holocene changes in the winds, upwelling and seasonal production of the northern California Current System, *Quat. Res., 38*, 359-370, 1992.

Sautter, L., and R. Thunell, Seasonal succession of the planktonic foraminifera: Results from a four year time-series sediment trap experiment in the northern Pacific, *J. Foraminiferal Res., 19*, 253-267, 1989.

Spigai, J.J., Marine geology of the continental margin off southern Oregon, Ph.D. thesis, 214 pp., Oregon State Univ., Corvallis, 1971.

Stuiver, M., and H.A. Polach, Reporting of ^{14}C data: A discussion, *Radiocarbon, 19*, 355-363, 1971.

Stull, R.B., *An Introduction to Boundary Layer Meteorology*, 666 pp., Norwell, Mass., 1988.

Zahn, R., T.F. Pedersen, B.D. Bornhold, and A.C. Mix, Water mass conversion in the glacial subarctic Pacific (54°N, 148°W): Physical constraints and the benthic- planktonic stable isotope record, *Paleoceanography, 6*, 543-560, 1991a.

Zahn, R., A. Rushdi, N.G. Pisias, B.D. Bornhold, B. Blaise, and R. Karlin, Carbonate deposition and benthic $\delta^{13}C$ in the subarctic Pacific: Implications for changes of the oceanic carbonate system, during the past 750,000 years, *Earth Planet. Sci. Lett., 103*, 116-132, 1991b.

S. Hostetler, U.S. Geological Survey at U.S. Environmental Protection Administration, Corvallis, OR 97330. (email: steve@sage.cgd.ucar.edu)

M. Kashgarian, Lawrence Livermore National Laboratory, Livermore, CA 92717. (email: kashgarian@LLNL.GOV)

A.C. Mix, College of Oceanic and Atmospheric Sciences, Oregon State University, Corvallis, OR 97331-5503. (email: amix@oce.orsat.edu)

J.D. Ortiz, Lamont-Doherty Earth Observatory of Columbia University, Palisades, NY 10964. (email: jortiz@ldeo.columbia.edu)

(Received November 29, 1995; revised September 30, 1996; accepted October 3, 1996)